Progress In Electromagnetics Research, Vol. 133, 53–89, 2013

PHASE-ONLY SYNTHESIS OF FLAT APERIODIC REFLECTARRAYS

A. Capozzoli[1, *], C. Curcio[1], A. Liseno[1], and G. Toso[2]

[1]Dipartimento di Ingegneria Biomedica, Elettronica e Delle Telecomunicazioni, Università di Napoli Federico II, Via Claudio 21, Napoli I 80125, Italy

[2]Antenna and Sub-Millimeter Wave Section, Electromagnetics Division, European Space Agency, Kepleerlan 1, PB 299, Noordwijk 2200 AG, The Netherlands

Abstract—A phase-only power pattern synthesis technique for flat (aperiodic) microstrip reflectarrays with elements arranged on a non-regular lattice is presented. The approach mitigates the typical design issues of reflectarray antennas related to the computational burden and to the possible occurrence of suboptimal solutions which are here even more significant due to the non-regular element lattice. This is done by a convenient two-stage procedure for choosing the starting point of the iterations and by proper representations of the unknowns of the problem. Design constraints on the element positions are also imposed to avoid overlapping as well as too large spacings. The algorithm, accelerated by parallel programming on Graphics Processing Units, has been analyzed against the cases of a pencil-beam and of a shaped-beam involving a typical South America coverage. In order to properly characterize the performance of the synthesis algorithm, it has been applied also to the design of reflectarrays with elements located on a non-regular lattice. The results show that in the case of non-regular lattice better directivities, better coverage behavior and better side-lobe levels are achievable as compared to reflectarrays characterized by a regular lattice.

1. INTRODUCTION

Microstrip reflectarrays are antennas made up of an aperture of microstrip patches scattering the incident field radiated by a feed horn according to given specifications on the beam shape [1].

Received 1 August 2012, Accepted 3 September 2012, Scheduled 17 October 2012

* Corresponding author: Amedeo Capozzoli (a.capozzoli@unina.it).

They combine some of the appealing features of microstrip patch arrays and reflectors [1, 2]. Like the former, they are low profile and lightweight. Like the latter, they provide high gains and do not require the use of cumbersome beamforming networks. Additionally, they are low cost, can be faceted or conformed [3, 4] and are aesthetically appealing for commercial applications.

Thanks to these features, reflectarrays have raised interest in many applications, as direct broadcast satellite (DBS) services [1], Earth remote sensing (requiring large apertures) [5] and in micro-spacecraft missions (requesting high gain antennas with small volume and low mass) [6], to mention just a few.

In many possible cases, as for satellite applications, high performance advanced reflectarray antennas are required satisfying complex and demanding design specifications [7].

In these instances, the desired control of the radiated pattern should, in principle, be achieved by exploiting all the possible degrees of freedom of the antenna on the one hand, and by considering an accurate pattern prediction model on the other hand.

A high number of degrees of freedom could be achieved by involving a high number of radiating elements, a high number of control parameters per element [8], including their positions [9–11, 13–16], and a purposely shaped reflecting surface [17, 23], possibly conformed around a specific shape in order to simplify deployability and installation [24].

Unfortunately, radiative models taking into account all the antenna degrees of freedom and exploiting the minimum number of approximations in the radiation operator [25] require accurate, efficient and effective design strategies. Indeed, higher accuracy means also higher computational burden and the use of an accurate model can, if not properly managed, make unaffordable the design of electrically large antennas. Throughout the literature, the approximate Phase-Only (PO) model [4, 26], although limiting the potentialities of the considered antenna, is often employed to reduce the number of involved parameters and make the design of the structure of interest less burdened. It consists in describing the dependence of the scattering matrix of each element on the features of the different patches by a factorized phase factor (henceforth addressed to as the "control phase" or "command phase") only and by a common vector term[†].

In addition, with reference to array antennas, the advantages of adopting a non-uniform element spacing in realizing an "equivalent

[†] It should be noticed that the PO model can be properly "tuned" to trade-off accuracy and efficiency. Indeed, the scattering model of each element described in [28] is "accurate", although the unknowns of the synthesis problem are still the element control phases.

tapering" or an array thinning, providing further degrees of freedom to the synthesis and thus helping satisfying the design specifications, have been reported since much time [9–12]. Opposite to this, in the framework of reflectarrays, and essentially due to computational issues, the antenna synthesis community has up to now mainly considered periodic lattices to enable the use of the "local periodicity" approximation [27] which, apart from possibly leading to locally significant errors, does not allow using at the best all the available degrees of freedom. Only since recently attempts to apply the equivalent tapering concept to reflectarray design are being performed [13–19].

It should be noticed that an aperture tapering could be in principle obtained by a proper feed system radiating the desired illuminating field, as suggested in [20, 21]. However, while the main benefits of reflectarrays stem from their simplicity, cheapness and low-mass profile (to be more easily included in satellite launches), a feed cluster would significantly increase the overall complexity, cost and weight, with also a worsening of the blocking efficiency [22]. Furthermore, unless using exceedingly large primary illuminators, an aperiodic reflectarray can reach a wide variety of (equivalent) amplitude tapers thanks to the possibility of exploiting a large number of degrees of freedom (in principle, the positions of all the reflectarray elements).

It is worth remarking that, besides coping with the above points, to improve accuracy and flexibility of the design process, the synthesis algorithm should evaluate the design parameters by satisfying, at the same time and with a reasonable accuracy, constraints drawn from the physics of the problem [29] as well as from the limitations of the electromagnetic model and from the physical realizability [30, 31].

The aim of this paper is to present an efficient and effective constrained PO approach [4, 32–34] for the power pattern synthesis of flat aperiodic reflectarrays. More in detail, the synthesis problem is formulated as an optimization one [37] and the approach aims at determining the control phases and the positions of the patch elements and enforces proper constraints on the element locations, a crucial point of such an application due to the need of guaranteeing adequate inter-element spacings [30–34]. The attention in this paper is focused on flat radiating structures and the performance of the approach is assessed against different test-cases comprising a pencil-beam as well as a shaped-beam. Due to the PO model, mutual coupling effects are not included. Once the command phases and element positions are determined, they are exploited as the starting point of a further optimization procedure, using a more accurate (not PO) radiation model accounting also for mutual coupling and which can be used to

refine the elements positioning and to obtain their internal parameters, see [18, 32, 33, 35, 36].

The paper is organized as follows. In Section 2, the reflector and array contributions to the reflectarray radiated field are introduced, allowing a very convenient modelling of aperiodic reflectarrays. In Section 3, the synthesis problem is formulated as an optimization one and the salient points of the synthesis strategy common to both the AS and APRPOS are briefly outlined. The AS and APRPOS stages are discussed in Sections 4 and 5, respectively, leaving some details in Appendix A and B. In Section 6, we illustrate how transforming the amplitude and phase distributions determined by the AS into a starting point for the APRPOS. Section 7 is devoted to a brief description of the algorithm implementations, while the results of the numerical analysis are provided in Section 8. Finally, Section 9 gathers the conclusions and the future developments.

2. *REFLECTOR* AND *ARRAY* CONTRIBUTIONS TO THE FIELD RADIATED BY AN APERIODIC REFLECTARRAY

In this section, we show how it is possible to identify the *reflector* and *array* contributions within the field scattered by a reflectarray.

To this end, we refer to the geometry of a flat aperiodic reflectarray shown in Fig. 1. The reflecting surface is illuminated by a primary source located at the origin of the Cartesian reference $Oxyz$ system and radiating a field $\underline{E}_f$. The reflectarray is made by N patches located on the $z = -z_0$ plane with (x_n, y_n) the coordinates of the n-th element.

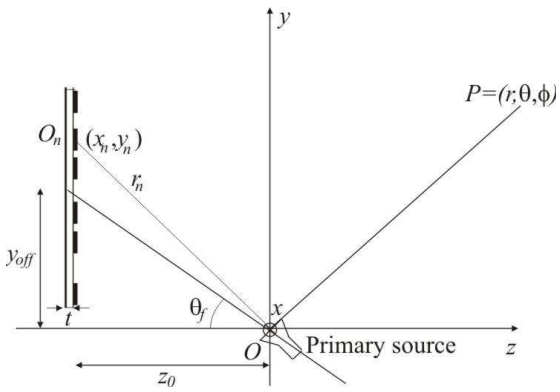

Figure 1. Geometry of the aperiodic reflectarray synthesis problem.

By applying the equivalence theorem to a volume excluding only the patches, the patches themselves can be suppressed and replaced by their respective induced electric current densities. Similarly, the illuminating structure can be represented by an equivalent current whose support can be assumed coincident with that of the feed itself. By applying the superposition principle, the radiated field can be calculated as the sum of two contributions, a first one, the *reflector* contribution, which is due to the feed density currents radiating in the presence of the dielectric slab and the ground-surface (Fig. 2(a)), and a second one, the *array* contribution, which is produced by the density currents induced on the patches, again in the presence of the slab plus ground plane. The second contribution can be calculated with a small approximation by using the spatial reflection theorem applied locally to the ground surface (Fig. 2(b)). It is completely independent of the patch arrangements and of their internal degrees of freedom and it changes only under a change of the ground shape. In the flat reflectarray case of interest in this paper, the ground contribution is not object of synthesis and can be calculated by means of a Geometrical Optics/Physical Optics approximation, as in standard reflectors [48, 49].

Formally, the relationship between the design parameters, i.e., the $N \times 2$ matrix $\underline{\underline{R}}$ defining the positions of the patches along with the $N \times M$ matrix $\underline{\underline{P}}$ of the M internal degrees of freedom of each patch,

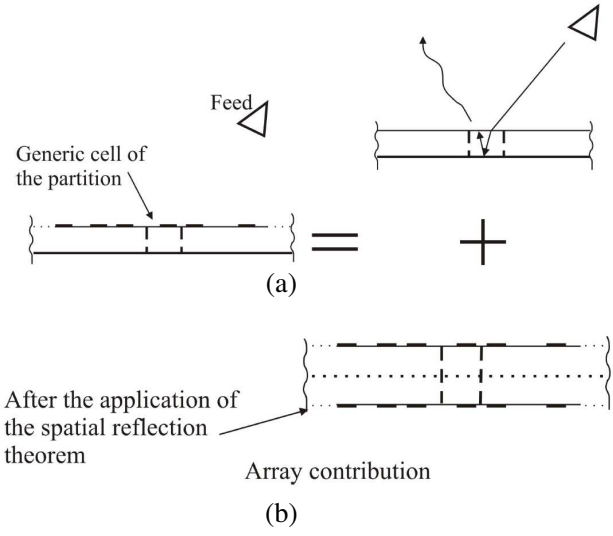

Figure 2. Illustrating the reflector and array contributions.

and the co-polar and cross-polar components of the far-field (E_{co}, E_{cr}) can be written as

$$\begin{cases} E_{co}(\underline{\underline{R}}, \underline{\underline{P}}) = E_{co}^{A}\left(\underline{\underline{R}}, \underline{\underline{P}}\right) + E_{co}^{R} \\ E_{cr}(\underline{\underline{R}}, \underline{\underline{P}}) = E_{cr}^{A}\left(\underline{\underline{R}}, \underline{\underline{P}}\right) + E_{cr}^{R} \end{cases} . \tag{1}$$

In Eq. (1), it has been explicitly highlighted that the array contribution depends on the internal degrees of freedom of the patches and on their arrangements on the reflecting surface and is object of synthesis in this paper. By the positions $\underline{\underline{R}}$, an "equivalent tapering" effect is achieved while, under the PO model to be detailed in Subection 5.1, the internal degrees of freedom $\underline{\underline{P}}$ are exploited to obtain the desired phase distribution over the reflectarray aperture. It should be noted that no other mean (e.g., passive or active elements, or couplings to the orthogonal polarization) is here employed to achieve a spatial taper over the reflectarray aperture.

3. THE SYNTHESIS STRATEGY

Since the high number of control parameters prevents from using global optimizations [38, 39], local, gradient-based searches are employed which, although computationally efficient, suffer from the local optima issue.

To face this point, the synthesis is performed by a pre-synthesis stage, henceforth the Aperture Synthesis (AS) stage, in which the amplitude and phase distributions of a continuous aperture are efficiently and effectively determined from the design specifications. Indeed, for this stage, the cost functional to be minimized is a fourth order polynomial in the unknown parameters, and so it is expected to provide a fast, robust (in terms of solution optimality) starting guess to the following stage [40].

The determined amplitude distribution is then interpreted as the equivalent tapering by which choosing the initial positions of the subsequent PO stage. The phase distribution, on the other side, dictates the initial command phase distribution of the patches.

During the subsequent Aperiodic Reflectarray Phase-Only Synthesis (APRPOS) stage, again to mitigate the false solution issue, the unknowns of the problem, i.e., the command phases and the element positions, are given proper representations enabling a progressive enlargement of the number of parameters to be determined as well as a modulation of the computational complexity of the approach [4, 32, 33]. Two steps are so devised. In the first step, few Zernike polynomials are employed for the command phases and progressively increased in number [4, 32, 33]. In the second step,

impulsive functions are adopted to represent the control phases individually [4, 32, 33]. In the APRPOS stage, to keep low the number of unknowns, a proper modal representation is introduced also for the element positions.

The details common to the two synthesis stages are now in order, while their peculiar aspects are discussed in Sections 4 and 5.

The purpose of each of the two synthesis stages is to find the unknown parameters, which change according to the stage and to the steps within the APRPOS stage, in order to satisfy the coverage requirements. The unknown parameters $\underline{\underline{R}}$ and $\underline{\underline{P}}$ should be obtained by minimizing a proper objective functional Φ given by:

$$\begin{aligned}\Phi\left(\underline{\underline{R}},\underline{\underline{P}}\right) &= \left\|A_{co}\left(\underline{\underline{R}},\underline{\underline{P}}\right) - P_{\mathcal{U}_{co}}\left(A_{co}\left(\underline{\underline{R}},\underline{\underline{P}}\right)\right)\right\|^2 \\ &\quad + \left\|A_{cr}\left(\underline{\underline{R}},\underline{\underline{P}}\right) - P_{\mathcal{U}_{cr}}\left(A_{cr}\left(\underline{\underline{R}},\underline{\underline{P}}\right)\right)\right\|^2 \end{aligned} \tag{2}$$

where (A_{co}, A_{cr}) is the relevant radiation operator which, according to Eq. (1), can be written as

$$\begin{cases} A_{co} = |E_{co}|^2 = \left|E_{co}^A\left(\underline{\underline{R}},\underline{\underline{P}}\right) + E_{co}^R\right|^2 \\ A_{cr} = |E_{cr}|^2 = \left|E_{cr}^A\left(\underline{\underline{R}},\underline{\underline{P}}\right) + E_{cr}^R\right|^2 \end{cases}. \tag{3}$$

$P_{\mathcal{U}_{co}}$ and $P_{\mathcal{U}_{cr}}$ are the metric projectors onto the set $\mathcal{U}_{co}$ and $\mathcal{U}_{cr}$ [41] that contain all the power patterns satisfying the specifications for the co-polar and cross-polar components, and $\|\cdot\|$ is a properly chosen norm. The sets $\mathcal{U}_{co}$ and $\mathcal{U}_{cr}$ are defined by mask functions (m_{co}, M_{co}) and (m_{cr}, M_{cr}), respectively, determining upper and lower bounds for A_{co} and A_{cr}, respectively [41]. The metric projectors $P_{\mathcal{U}_{co}}(A_{co})$ and $P_{\mathcal{U}_{cr}}(A_{cr})$ are defined as [41]

$$P_{\mathcal{U}_{co,cr}}(A_{co,cr}) = \begin{cases} m_{co,cr} & \text{if } A_{co,cr} \le m_{co,cr} \\ A_{co,cr} & \text{if } m_{co,cr} \le A_{co,cr} \le m_{co,cr} \\ M_{co,cr} & \text{if } M_{co,cr} \le A_{co,cr} \end{cases}. \tag{4}$$

For the cases of interest in this paper, Φ will refer only to the co-polar term and only the A_{co} operator (which will be changed according to the involved step) will be relevant to our purposes.

4. APERTURE SYNTHESIS (AS)

Let us consider a rectangular aperture $D_{ap} = [-a_{ap}, a_{ap}] \times [-b_{ap}, b_{ap}]$, lying in the xy plane of a cartesian coordinate system $Oxyz$ and radiating towards the $z > 0$ half-space.

The size, shape and polarization of the aperture are chosen according to the specifications on the reflectarray dimensions and shape and on the particularly dealt with radiating elements. In this paper,

according to the considered patches, the aperture field $\underline{E}_a$ is assumed to be linearly polarized along the y-axis, i.e., $\underline{E}_a = E_a \hat{i}_y$. The aperture field distribution $E_a(x, y)$ is the unknown to be determined and is represented by means of properly chosen expansion functions [42].

In order to choose such functions, let us observe that the component $\hat{E}(u, v)$ of the Plane Wave Spectrum (PWS) homologous to E_a can be written as

$$\hat{E}(u,v) = \iint_{D_{ap}} E_a(x,y) e^{j\beta(ux+vy)} dxdy = \mathcal{F}_{D_{ap}}[E_a], \quad (u,v) \in \Omega \quad (5)$$

where $\beta = 2\pi/\lambda$ is the wavenumber, λ being the wavelength, $\mathcal{F}_{D_{ap}}$ the Fourier transform operator truncated to D_{ap}, and Ω the region of the (u, v) plane wherein the design specifications are enforced. For the AS stage, the specifications are enforced on $\hat{E}$ so that functional (2) is optimized by letting $A_{co} = |\hat{E}|^2$. On choosing hereinafter the $L^2(\Omega)$ norm for the functional (2), to effectively represent E_a (i.e., to represent E_a with the least number of functions), the expansion functions should account for both the information on shape and size of the aperture and of the spectral region Ω. Let us then define $\bar{\Omega} = [-\bar{u}, \bar{u}] \times [-\bar{v}, \bar{v}]$ the smallest rectangle containing Ω. For example, when Ω is the entire visible region, $\bar{u} = \bar{v} = 1$. Then the ϕ_{mn}'s should be functions with support limited to D_{ap} and band-limited to the $\bar{\Omega}$. In other words, they should be chosen as Prolate Spheroidal Wave Functions (PSWFs) [42–44], i.e.,

$$E_a(x,y) = \sum_{m=0}^{M} \sum_{n=0}^{N} a_{mn} \Phi_m[c_x, x] \Phi_n[c_y, y], \quad (6)$$

where $\Phi_i[c_w, w]$ is the i-th one-dimensional PSWF with "space-bandwidth" product c_w, $c_x = \beta \bar{u} a_{ap}$, and $c_y = \beta \bar{v} b_{ap}$. The a_{mn}'s are expansion coefficients to be determined according to the design specifications, by taking into account that $\hat{E}$ is related to the a_{mn}'s via Eqs. (5) and (6).

In the case of pencil-beams, the determination of the a_{mn}'s can be carried out by exploiting results of convex optimization [45–47].

On the other side, in the case of either pencil-beams or shaped-beams, the determination of the a_{mn}'s can be performed in an efficient and reliable way by a *quadratic* approach, since the equivalent tapering concept can be exploited for the step in Section 5. Indeed, the radiation operator A_{co} in Eq. (2) is linearly related to the a_{mn}'s, so that the functional Φ is a fourth-order polynomial in the unknown parameters, i.e., is related to the a_{mn}'s with the lowest possible degree of non-linearity [40, 42]. This, along with the opportunity of performing a

progressive enlargement of the unknown space, is known to have a positive effect on the trapping problem [40, 42].

In Section 7, we will show that the two mentioned schemes provide quite similar results in the case of pencil-beams, so that the quadratic approach will be selected, in this paper, to construct the starting point of the APRPOS stage for both, the pencil-beam and shaped-beam cases.

5. APRPOS

In this stage, the unknowns of the problem are the command phases of each reflecting element and the element positions on the reflectarray surface.

In the following, the details concerning this synthesis stage are provided.

5.1. The PO Radiating Model

Let us denote by (r, θ, ϕ) the spherical coordinates of an observation point P located in the far-zone of the reflectarray.

On assuming each patch to be located in the far-zone of the primary source, then the far-field pattern of the reflectarray can be written as

$$\begin{pmatrix} F_{co} \\ F_{cr} \end{pmatrix}(u,v) = \underline{\underline{Q}}(u,v) \sum_{n=1}^{N} \underline{\underline{S}}^{A}_{n}(u,v) \underline{E}_{f_n} e^{j\beta(ux_n+vy_n)} + \begin{pmatrix} F^R_{co} \\ F^R_{cr} \end{pmatrix}(u,v) \tag{7}$$

where

- F_{co} and F_{cr} are the co-polar and cross-polar components of the far-field pattern, respectively:

$$\begin{pmatrix} E_{co} \\ E_{cr} \end{pmatrix} = \frac{e^{-j\beta r}}{r} \begin{pmatrix} F_{co} \\ F_{cr} \end{pmatrix}; \tag{8}$$

- the first term on the right hand side represents the array contribution while the second term represents the reflector contribution;
- u and v in the visible region are related to θ and ϕ by the well known relations $u = \sin\theta\cos\phi$, $v = \sin\theta\sin\phi$;
- $\underline{\underline{S}}^{A}_{n} = \begin{bmatrix} S^A_{xx_n} & S^A_{xy_n} \\ S^A_{yx_n} & S^A_{yy_n} \end{bmatrix}$ is the scattering matrix of the n-th element expressed in terms of the Cartesian components, related to the array contribution [25];

- $\underline{E}_{f_n} = \left(\underline{E}_{\,f}(x_n, y_n, -z_0) \cdot \hat{i}_x, \underline{E}_{\,f}(x_n, y_n, -z_0) \cdot \hat{i}_y\right)^T$;
- $\underline{\underline{Q}}$ is the matrix converting the Cartesian components in the $\underline{\underline{O}}xyz$ system of the scattered field to the co-polar and cross-polar components of the reflectarray far-field;
- F_{co}^R and F_{cr}^R are the co-polar and cross-polar components of the far-field pattern of the reflector contribution, respectively.

Unfortunately, a direct application of the PO approach to the array terms $\underline{\underline{S}}_{\,n}^A(u,v)$ can be either not possible, for example because the amplitudes of the elements of $\underline{\underline{S}}_{\,n}^A(u,v)$ do not keep approximately constant, or cumbersome. Indeed, in cases when it is possible, the phase of $\underline{\underline{S}}_{\,n}^A(u,v)$ might not range between 0° and 360°, thus compelling to the use of a constrained synthesis or to the introduction of nonlinear relations to ensure the final command phase to range within the prescribed interval.

Actually, we are now showing that [4, 32, 33], also in the aperiodic case, a scattering matrix $\underline{\underline{S}}_{\,n}$ can be introduced so that Eq. (7) turns into

$$\begin{pmatrix} F_{co} \\ F_{cr} \end{pmatrix}(u,v) = \underline{\underline{Q}}(u,v) \sum_{n=1}^{N} \underline{\underline{S}}_{\,n}(u,v) \underline{E}_{\,f_n} e^{j\beta(ux_n + vy_n)} \tag{9}$$

and can be approximately expressed as the sum of two contributions, one due to the dielectric slab and the ground plane (*reflector* contribution), and one due to the presence of the corresponding patch (*array* contribution), scattering in presence of the reflector, see the details in Appendix A. In other words

$$\underline{\underline{S}}_{\,n}(u,v) = \underline{\underline{S}}_{\,n}^A(u,v) + \underline{\underline{S}}_{\,n}^R(u,v). \tag{10}$$

Let us observe that, in general, it is more advantageous to write also the reflector contribution as a summation of different terms and the approach that has resulted the most convenient to our purposes is reported in the following.

In a partitioning dictated by the patch positions, one could conclude that, by changing the patch positions, the portion of ground subtended by each patch, and thus the overall ground partitioning, would be modified. Nevertheless, it is possible to observe that:

- the overall reflector contribution due to all the cells forming the partitioning is independent of the patch positions (see Appendix B) and can be evaluated by using a Geometrical Optics/Physical Optics approach, as in standard reflectors [48, 49]; it remains the same for a fixed size of the ground plane, independently of the patch positioning;

- the overall reflector contribution can be subdivided as the sum of different contributions $\underline{\underline{S}}_n^R$'s corresponding to the part of the ground plane centered around the n-th patch, even in the case of overlapping partitioning (see Appendix B); indeed, in the direction of the main beam (assumed to be the specular one), each of them can be approximately considered as independent of the position of the corresponding patch and thus of the mentioned partitioning, including the overlapping; in other words, it is possible to approximate it by a "mean" contribution, according to Appendix B, so that $\underline{\underline{S}}_n^R \simeq \underline{\underline{S}}^R$.

In this way, the subscript n in the definition of $\underline{\underline{S}}_n$ highlights the dependence of the scattering matrix on

- $\underline{p}_n = (p_{n_1}, p_{n_2}, \ldots, p_{n_L})$ representing the vector of the L control parameters of the n-th patch;
- the cosine directors of the impinging directions of the primary field $u_n = \frac{O_n - O}{|O_n - O|} \cdot \hat{i}_x$ and $v_n = \frac{O_n - O}{|O_n - O|} \cdot \hat{i}_y$.

Equation (9) can be simplified, by neglecting some of the involved dependencies and by exploiting the PO scattering model [4, 26, 32, 33]. Indeed, if the radiating elements and the feed are not electrically large, the angle under which the primary field impinges on the reflectarray elements can be assumed to be the same for all the patches so that the dependence of the scattering matrix from u_n e v_n can be neglected.

Moreover, and according to the PO model, the dependence of the $\underline{\underline{S}}_n$'s on the features of the different patches can be lumped in a phase factor $\exp(j\psi_n)$ only and in a term $\underline{\underline{S}}_0$ common to all the $\underline{\underline{S}}_n$'s, that is, $\underline{\underline{S}}_n(u, v) = \underline{\underline{S}}_0(u, v)\exp(j\psi_n)$. The validity of the PO model is illustrated in Fig. 3 showing the approximately constant behavior of the amplitude of S_{yy} for the common case of a rectangular patch. On the other side, Fig. 4 depicts the behavior of the command phase in the same circumstances of Fig. 3. As it can be seen, the command phase ranges approximately between 0° and 360°, thus avoiding the need of applying any range constraints to the ψ_n's or non-linear transformations.

Following a PO synthesis stage, each patch can be approximately assigned its corresponding command phase by choosing the resonant length according to Fig. 4. Numerical simulations have indicated that the radiation of reflectarrays synthesized by the APRPOS have already a good degree of matching with the radiation of the same reflectarray as evaluated by the more "accurate" model in Eq. (9) [18]. Such a solution can be nevertheless refined by a further synthesis stage, relying on Eq. (9), which is however beyond the scope of the present paper.

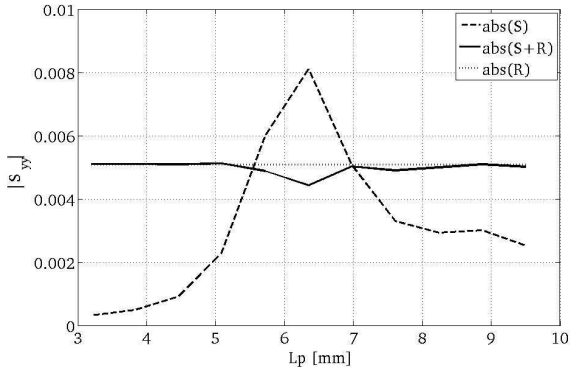

Figure 3. Absolute value of the contributions to S_{yy} for different resonating lengths L_p of the rectangular patch. Solid line: $|S_{yy}|$. Dashed line: $|S^A_{yy}|$. Dotted line: $|S^R_{yy}|$. Substrate of relative permittivity 2.5 and thickness 0.762 mm (Arlon DiClad 527), $(u_n, v_n) = (-0.1003, -0.2309)$.

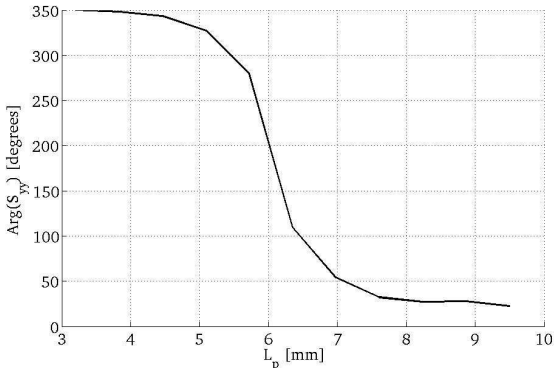

Figure 4. Control phase for different resonating lengths L_p of the rectangular patch. Substrate of relative permittivity 2.5 and thickness 0.762 mm (Arlon DiClad 527), $(u_n, v_n) = (-0.1003, -0.2309)$.

Accordingly, $\underline{E}_f$ can be approximated as

$$\underline{E}_{f_n} \simeq \underline{\tilde{E}}_f w_n^{m_f} \frac{e^{-j\beta r_n}}{r_n} \tag{11}$$

where $\underline{\tilde{E}}_f$ is a vector independent on the index n [4], $w_n = \sqrt{1-u_n^2-v_n^2}$, $r_n = |O_n - O|$ and a $w_n^{m_f}$ type pattern has been

assumed.

Summarizing, Eq. (9) can be rewritten as

$$\begin{pmatrix} F_{co} \\ F_{cr} \end{pmatrix}(u,v) = \underline{\underline{Q}}(u,v)\underline{\underline{S}}_0(u,v)\underline{\tilde{E}}_f \sum_{n=1}^{N} w_n^{m_f} \frac{e^{-j\beta r_n}}{r_n} e^{j\psi_n} e^{j\beta(ux_n+vy_n)}. \quad (12)$$

that is, as the product between an "element factor" $\underline{\underline{Q}}(u,v)\underline{\underline{S}}_0(u,v)\underline{\tilde{E}}_f$ and an "array factor"

$$F(u,v) = \sum_{n=1}^{N} w_n^{m_f} \frac{e^{-j\beta r_n}}{r_n} e^{j\psi_n} e^{j\beta(ux_n+vy_n)} \quad (13)$$

containing the control phases ψ_n useful for the beam shaping and to be determined by the synthesis algorithm along with the element positions. Functional (2) is then applied in this stage with $A_{co} = |F_{co}|^2$. In this way, the speedup [55] required by a stage appointed to quickly provide a solution to be eventually and subsequently refined is obtained.

5.2. Representation of the Unknowns

5.2.1. Representation of the Element Positions

Regarding the element locations, let us observe that directly exploiting the coordinates (x_n, y_n) as optimization variables has three main drawbacks. The first one is related to the number of the involved parameters, which would be equal to twice the total number of patches N. The second one is due to the difficulty of devising an efficient strategy to enforce constraints on the minimum and maximum element spacings, without significantly burdening the optimization. The third one concerns the impossibility of performing a progressive enlargement of the unknowns.

To this end, proper mapping functions transforming uniform 2D lattices into non-uniform ones are employed to represent the patch locations by a prefixed number of parameters [30, 31]. In this way, the positions (x_n, y_n) are represented as

$$(x_n, y_n) = \left(h\left(t_n^{(1)}, t_n^{(2)}\right), g(t_n^{(1)}, t_n^{(2)}\right)\right), \quad (14)$$

with

$$h\left(t_n^{(1)}, t_n^{(2)}\right) = \sum_{r=1}^{R}\sum_{s=1}^{S} \alpha_{rs} L_r\left(t_n^{(1)}\right) L_s\left(t_n^{(2)}\right), \quad (15)$$

and

$$g\left(t_n^{(1)}, t_n^{(2)}\right) = \sum_{r=1}^{R}\sum_{s=1}^{S} \beta_{rs} L_r\left(t_n^{(1)}\right) L_s\left(t_n^{(2)}\right), \tag{16}$$

where $(t_n^{(1)}, t_n^{(2)})$ defines a uniform lattice in the square $(-1,1) \times (-1,1)$. L_j is a properly defined set of basis functions (e.g., Legendre polynomials, as employed in the numerical analysis), and α_{rs} and β_{rs} are proper expansion coefficients.

The functions h and g serve to map a uniform lattice of $(-1,1) \times (-1,1)$ to a non-uniform lattice of the (x,y) plane. Instead of representing the individual position of each element, which implies dealing with a large (N) number of unknowns, the patch locations are obtained by the specifying the α_{rs} and β_{rs}. This point is pictorially illustrated, for the 1D case, in [30, 56]. The representation in Eqs. (14), (15) and (16) is able to significantly reduce the number of the parameters to be sought for during the optimization of Φ, as the actual unknowns of the procedure reduce to a few coefficients α_{rs} and β_{rs} [30, 31]. In this way, the computational complexity is reduced. In the Authors' experience, and consistently with the results in [57, 58], a reduction of the number of unknowns strengthens, for the functional at hand, the approach against the local minima problem by a progressive increase of the number of unknowns.

5.2.2. Representation of the Element Command Phases

Concerning now the phase representations, let us observe that, starting from the initial point provided by the AS (see Section 5), the first step of the APRPOS stage is aimed at returning a reliable, although rough, determination of the control phases. To this end, only a reduced number of degrees of freedom, and thus of the unknowns to be searched for, are involved. This is accomplished by representing the ψ_n's by low order Zernike polynomials Z_t, i.e.,

$$\psi_n = \sum_t c_t Z_t\left(t_n^{(1)}, t_n^{(2)}\right). \tag{17}$$

The second step provides the ultimate solution by setting $\psi_n = \delta(x - x_n, y - y_n)$, so considering all the degrees of freedom of the structure, since the unknowns now coincide with the control phases [4, 32, 33].

6. FROM AS TO APRPOS

Following Eq. (12) and the involved approximations, the reflectarray can be dealt with as an array to all intents and purposes, and so all

the tools of array synthesis can be exploited. Such an array has a PO control, unless the element positions do not represent a further degree of freedom to achieve an "equivalent spatial tapering".

The starting point of the APRPOS is then chosen following the AS result, according to a two-steps procedure. The first step is to turn the aperture field amplitude distribution into an "equivalent spatial tapering" giving a starting guess for the patch positions. The second step is to turn the aperture field phase distribution into a starting guess for the command phases.

Irregularly spacing array elements to provide an "equivalent spatial tapering" has been firstly faced by Doyle [50] and Skolnik [51] for the 1D case. The underlying idea is to arranging equally excited elements so that by their "spatial density" the current of a continuous aperture radiating a field satisfying the specifications is approximated. Recently, the work by Doyle and Skolnik has been improved [52, 53], but these techniques hold only for 1D arrays, whereas the radiating structure we are dealing with is 2D. Accordingly, a different procedure should be used here, but taking into account that it should provide a rough initial guess to be subsequently refined by the APRPOS stage.

The idea is to choose the inter-element patch spacings according to the reciprocal of the amplitude $A = |E_a|$ of the aperture field distribution determined by the AS. In this way, the more the aperture amplitude taper (the lower the field amplitude) the larger the spacing. This is roughly obtained by fixing the inter-element spacings along the x- and y-axes according to the solution of the following differential equations

$$\frac{\partial x(\xi,\eta)}{\partial \xi} = \frac{C(\eta)}{\bar{A}(\xi,\eta)} + D(\eta) \tag{18}$$

$$\frac{\partial y(\xi,\eta)}{\partial \eta} = \frac{G(\xi)}{\bar{A}(\xi,\eta)} + H(\xi), \tag{19}$$

where a proper threshold is applied to A to avoid an exceedingly large spacing, obtaining $\bar{A}$. The auxiliary functions $C(\eta)$, $D(\eta)$, $G(\xi)$ and $H(\xi)$ are needed to enforce minimum and maximum tolerable spacings [17, 18]. Eqs. (18) and (19) represent a rough generalization to the 2D case of the 1D approach in [30, 31]. Note that, the procedure is consistent since, when $\bar{A}$ is large, then an approximately uniform spacing is obtained since in this case $\partial x/\partial \xi \simeq D(\eta)$ and $\partial x/\partial \eta \simeq H(\xi)$. On the other side, when $\bar{A}$ is small, then $\partial x/\partial \xi \simeq C(\eta)/\bar{A}(\xi,\eta)$ and $\partial y/\partial \eta \simeq G(\eta)/\bar{A}(\xi,\eta)$.

By defining (ξ_n, η_m) as an uniform grid of D_{ap} with spacings $\Delta\xi$ and $\Delta\eta$, Eqs. (18) and (19) can be discretized so that the (x_{nm}, y_{nm})

coordinates are obtained by solving the difference equations

$$x_{n+1,m} - x_{n,m} = \left[\frac{C_m}{\bar{A}(\xi_n, \eta_m)} + D_m\right] \Delta\xi \tag{20}$$

$$y_{n,m+1} - y_{n,m} = \left[\frac{G_n}{\bar{A}(\xi_n, \eta_m)} + H_n\right] \Delta\eta \tag{21}$$

The constants C_m and D_m are then chosen as

$$\begin{cases} C_m = \dfrac{d_{\max} - d_{\min}}{\dfrac{1}{\min_n \bar{A}(\xi_n, \eta_m)} - \dfrac{1}{\max_n \bar{A}(\xi_n, \eta_m)}} \dfrac{1}{\Delta\xi} \\ D_m = \left[d_{\max} - d_{\min} \dfrac{\max_n \bar{A}(\xi_n, \eta_m)}{\min_n \bar{A}(\xi_n, \eta_m)}\right] \dfrac{1}{\Delta\xi} \end{cases}, \tag{22}$$

where $d_{\min}$ and $d_{\max}$ denote the minimum and maximum allowed inter-element spacings, respectively. G_n and H_n have analogous expressions.

Following the previous step, the initial command phases are chosen, starting from the phase of the aperture distribution determined by the AS, according to the following procedure.

We consider the pattern radiated by the aperture discretized at the (ξ_n, η_n) points, that is,

$$F_{unif}(u, v) = \sum_{n=1}^{N} A(\xi_n, \eta_n) e^{j\Psi_n} e^{j(\xi_n u + \eta_n v)} \tag{23}$$

where the Ψ_n's are the samples of the aperture field phase. Next, we consider the array factor in Eq. (13) and compare it to (23). We then choose the command phases ψ_n's so that, around the center (u_0, v_0) of the main beam, the phase of each of the terms in Eqs. (13) and (23) coincide. In other words, we set

$$\psi_n = \Psi_n + u_0(\xi_n - x_n) + v_0(\eta_n - x_n) + \beta r_n. \tag{24}$$

7. ALGORITHM IMPLEMENTATION

The algorithm has been implemented in a Matlab script and made computationally efficient as the radiated field and the functional gradients for the APRPOS stage are computed by Non-Uniform Fast Fourier Transform (NUFFT) routines (whose asymptotic computational burden is comparable to that of standard FFT routines) [54] and by proper parallel implementations on a GPU in CUDA language [55, 59].

The processing has been performed on a Genesis Tesla I-7950 workstation, with a 8-core Intel CPU i7-950, working at 3.06 GHz and

with 6 GB of RAM. The workstation is equipped with an Nvidia Tesla C2050, benefitting of the state-of-the-art Fermi GPU architecture and consisting of 14 streaming multiprocessors (SMs), each containing 32 streaming processors (SPs), or processor cores, running at 1.15 GHz. The C2050 is further equipped with a 2.8 GB, off-chip, global memory and supports double precision arithmetics.

7.1. Optimization

Both during the AS and the APRPOS stages, the projection $P_{\mathcal{U}_{co}}(|A_{co}|^2)$ is evaluated and fixed and the functional Φ optimized. Subsequently, a new projection is evaluated and fixed and Φ optimized once again iteratively.

Concerning the AS, minimization by the Polak-Ribiére scheme is employed [40, 42, 60]. Thanks to the fourth-order nature of the functional for this stage, the line minimization is performed in an "exact" way and it is very fast to be computed [60].

Regarding the APRPOS, the minimization is performed by the Matlab function *fmincon*. In order to avoid computationally burdened optimizations, at each iteration step, two different minimizations are performed, one involving the command phases only and one involving the patch positions only.

7.2. Efficient Evaluation of the Radiation Operator and Functional Gradient for the AS and APRPOS Stages

To limit the burden, it is necessary to effectively evaluate both the radiated field and the gradient of Φ for the two stages.

For the AS, Eq. (5) can be effectively performed by standard FFT routines. On the other side, the functional gradient can be calculated observing that

$$\frac{\partial \Phi}{\partial a_{mn}^R} = 16\pi^2 \,\mathrm{Re}\left\{\left\langle \phi_{mn}, \mathcal{F}_{\bar{\Omega}}^{-1}\left[w\hat{E}\left(|\hat{E}|^2 - P_{\mathcal{U}_{co}}\left(|A_{co}|^2\right)\right)\right]\right\rangle\right\} \quad (25)$$

and that

$$\frac{\partial \Phi}{\partial a_{mn}^I} = 16\pi^2 \,\mathrm{Im}\left\{\left\langle \phi_{mn}, \mathcal{F}_{\bar{\Omega}}^{-1}\left[w\hat{E}\left(|\hat{E}|^2 - P_{\mathcal{U}_{co}}\left(|A_{co}|^2\right)\right)\right]\right\rangle\right\}, \quad (26)$$

where a_{mn}^R and a_{mn}^I denote the real and imaginary parts, respectively, of the expansion coefficients a_{mn}'s in Eq. (6), $\langle\cdot\rangle$ represents the scalar product in $\mathcal{L}^2(D_{ap})$ and $\mathcal{F}_{\bar{\Omega}}^{-1}$ represents the inverse Fourier transform limited to $\bar{\Omega}$. The derivatives in Eqs. (25) and (26) can be again effectively evaluated by standard FFT routines [60].

Regarding the radiation operator for the APRPOS, NUFFT routines have been adopted to cope with the irregular spacing, see [55].

Concerning the functional gradient, when a representation in terms of Zernike polynomials is adopted and thanks to representations (15), (16) and (17) significantly limiting the number of unknowns, the gradient of Φ with respect to the α_{rs}'s, β_{rs}'s and c_t's, is evaluated by finite differences. Opposite to this, when a representation of the control phases in terms of "pulse" basis functions $l_k(x,y) = \delta(x - x_k, y - y_k)$ is adopted, the gradient can be effectively evaluated by the relation

$$\frac{\partial \Phi}{\partial \psi_k} = -4\,\mathrm{Im}\left\{ f_k e^{j\psi_k} \sum_{h=1}^{H} E^*_{co_h} \left(|F_{co_h}|^2 - |(P_{\mathcal{U}_{co}}(|F_{co_h}|^2))_h|^2 \right) g_h e^{j[u_h x_k + v_h y_k]} \right\} \tag{27}$$

where (u_h, v_h) is one of the H spectral points of interest, g_h the co-polar term of $\underline{\underline{Q}}\,\underline{\underline{S}}_0\underline{\tilde{E}}_f$, and $f_k = w_k^{m_f}\theta_k \exp(j\psi_k)\exp(-j\beta r_k)/r_k$. The derivatives in Eq. (27) can be evaluated again by means of a single NUFFT routine call.

8. RESULTS

In this section, we present numerical results to show the performance of the proposed approach.

The results refer to two different kinds of beams, namely, to a (tilted) pencil-beam and to a shaped-beam involving a typical South America coverage. The working frequency has been 14.25 GHz. For all the considered test-cases, the upper co-polar mask has been assumed to be $+0.5$ dB within the coverage and -35 dB outside. On the other side, the lower copolar mask has been assumed to be -0.5 dB within the coverage and -100 dB outside. Furthermore, constrained syntheses have been considered with minimum and maximum allowed spacings equal to 0.5λ and 0.7λ, respectively. Too small spacings must indeed be avoided, to avoid complex interactions among adjacent elements preventing to treat them separately and to obviously avoid overlappings among neighbor patches [30, 31]. Also constraints on the maximum spacing are necessary, to avoid exceedingly large gaps between the elements [30, 31] giving rise to large reflections from the reflectarray substrate and ground plane.

To highlight the benefits arising from the use of a non-uniform element positioning, the results are compared to those achievable with a uniform, $\lambda/2$ element spacing.

During the presentation of the results, attention will be given to the construction of the starting point. Indeed, in the Authors' experience, the choice of the initial guess by the procedure detailed in Sections 2 and 5 is very important to obtain a satisfactory result.

For the shaped beam test case, the overall processing time has been of about four hours on the computing platform indicated in Section 7.

8.1. Synthesis of a Tilted Pencil-beam

The main antenna parameters for this test case are summarized in Table 1 (see also Fig. 1). The antenna has been synthesized to radiate a pencil beam in the direction $(u_0, v_0) = (0, 0.40)$, i.e., in the specular direction of the primary field.

Before showing the obtained results, let us stick on the construction of the initial guess for the APRPOS stage. More in detail, we want to compare, for the case of pencil-beams, the result achievable by using a linear (convex) programming scheme [46], not suffering from the local minima issue, and the AS one. Such a comparison is performed in Fig. 5. For the sake of simplicity, a 20×20 array has been considered, radiating a centered beam. The array spacing is uniform and equal to $\lambda/2$ for the technique in [46], while the aperture

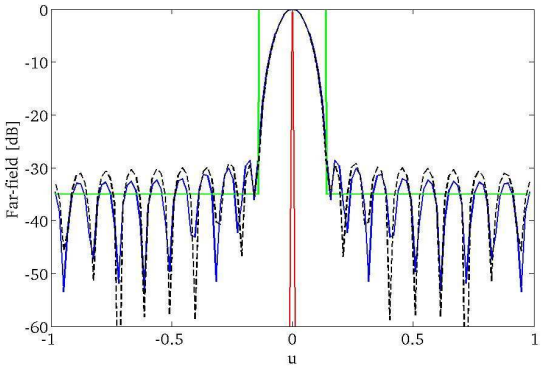

Figure 5. Comparison between the cuts, along the u-axis, of the pencil beam pattern radiated by a uniform, 20×20 array ($\lambda/2$ spacing) synthesized by the linear programming approach in [46] (dashed black line) and that achieved by the described AS scheme (solid blue line). The green and red line show the upper and lower mask functions, respectively, which have been applied to the AS.

Table 1. Main parameters for the tilted pencil-beam test-case.

Number of elements	30×30
y_{off}	8.25λ
z_0	8.48λ
$\theta_f = a\tan(y_{off}/z_0)$	$44°$
Minimum allowed spacing	0.5λ
Maximum allowed spacing	0.7λ

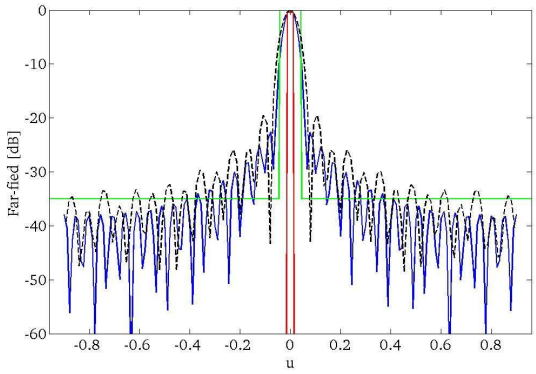

Figure 6. Cut, along the $v = 0.4\beta$-axis, of the pencil beam pattern radiated by the synthesized, 30×30 aperiodic reflectarray (solid blue line) as compared to that radiated by the synthesized, 30×30 periodic ($\lambda/2$ spacing) reflectarray (dashed black line). The green and red line show the upper and lower mask functions, respectively, which have been applied to both the cases.

field distribution obtained by the AS stage has been sampled with the same $\lambda/2$ rate. The target beam-width has been 10°, while the target Side Lobe Level (SLL) has been -30 dB. As it can be seen, the two approaches have a similar performance, which highlights the robustness of the AS scheme against the sub-optimal solutions and justifies its use to construct the starting point.

Let us now turn the attention to the final result of the APRPOS stage. In Figs. 6 and 7, the cuts along the $v = 0.4$- and v-axes, respectively, of the far-field patterns radiated by the synthesized aperiodic reflectarray are presented and compared to the outcomes of the corresponding periodic case. As it can be seen, the aperiodic synthesis outperforms the periodic one, both in terms of main beam-

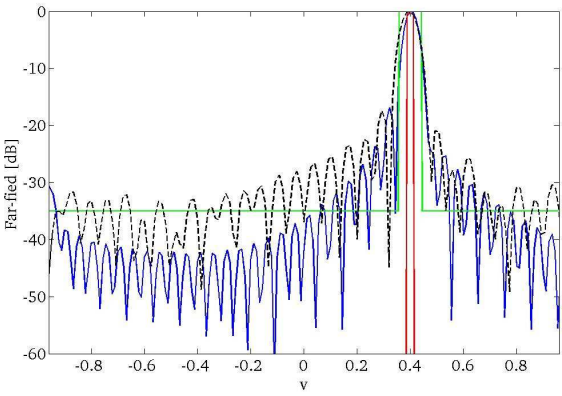

Figure 7. Cut, along the v-axis, of the pencil beam pattern radiated by the synthesized, 30×30 aperiodic reflectarray (solid blue line) as compared to that radiated by the synthesized, 30×30 periodic ($\lambda/2$ spacing) reflectarray (dashed black line). The green and red line show the upper and lower mask functions, respectively, which have been applied to both the cases.

width and of side-lobe behavior. To state this more quantitatively, we mention that the maximum directivity for the aperiodic case has been 35.51 dBi, which is better than that for the periodic case, resulted equal to 33.8 dBi. The increase in directivity reported in Figs. 6 and 7 of the aperiodic reflectarray as compared to the periodic case has been obtained thanks to the use of the irregular elements positioning (not shown here for the sake of brevity). In [34], the results achievable by the described aperiodic synthesis tool have been compared to those obtained by the same tool as applied to the design of two periodic reflectarrays, one having the same number of elements of the aperiodic one, regularly positioned so to allow the same aperture, and the other having elements spaced half a wavelength. The performance of the aperiodic reflectarray has outperformed that of both the periodic ones. For the sake of completeness, in Figs. 8 and 9, the aperiodic result is compared to the starting point determined from the AS following the procedure in Section 5. For the aperiodic case, the synthesized command phases are displayed in Fig. 10. The minimum and maximum inter-element spacings have been 0.55λ and 0.7λ, respectively. We have verified that the result of the periodic synthesis has better performance than a reflectarray obtained by a simple PO control of the beam pointing direction through a phase tilt.

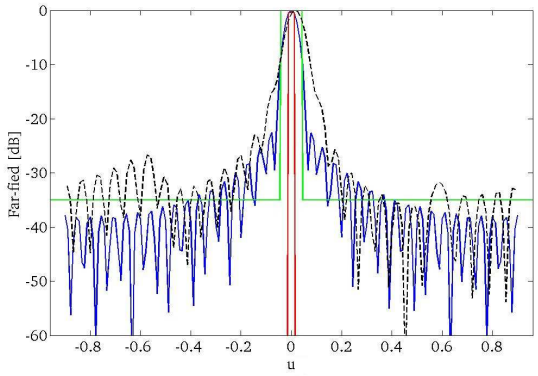

Figure 8. Cut, along the $v = 0.4\beta$-axis, of the pencil beam pattern radiated by the synthesized, 30×30 aperiodic reflectarray (solid blue line) as compared to the starting point determined from the AS following the procedure in Section 5 (dashed black line). The green and red line show the upper and lower mask functions, respectively.

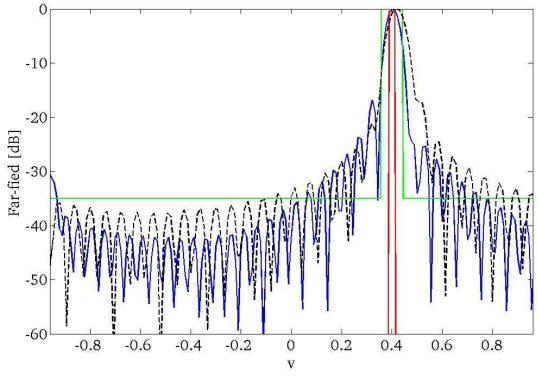

Figure 9. Cut, along the v-axis, of the pencil beam pattern radiated by the synthesized, 30×30 aperiodic reflectarray (solid blue line) as compared to the starting point determined from the AS following the procedure in Section 5 (dashed black line). The green and red line show the upper and lower mask functions, respectively.

Finally, as a further advantage of the irregular element positioning, we want to remark that the same approach, but based on a proper multi-frequency formulation, allows to optimize the antenna behavior over a certain bandwidth. Results concerning improvements on the

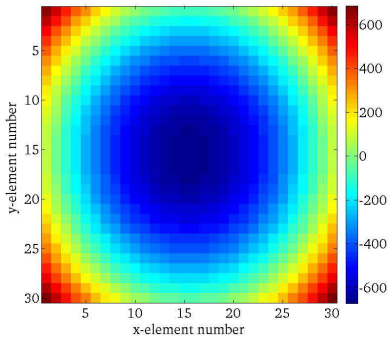

Figure 10. Control phases for the synthesized, 30×30 aperiodic reflectarray.

Table 2. Main parameters for the South America coverage test-case.

Number of elements	51×51
y_{off}	13.75λ
z_0	28.28λ
$\theta_f = a\tan(y_{off}/z_0)$	$26°$
Minimum allowed spacing	0.4λ
Maximum allowed spacing	0.7λ

bandwidth behavior of the aperiodic reflectarray against a single-frequency synthesis for the case of pencil beams are reported in [61].

8.2. Synthesis of a Shaped Beam with South America Coverage

We now show results concerning the synthesis of a 51×51 shaped-beam reflectarray radiating according to the typical South America coverage. The coverage masks have been generated by assuming a geostationary satellite reflectarray with position $67E0N$ and the main antenna parameters for this test-case are summarized in Table 2.

To start with, Figs. 11 and 12 show the amplitude and phase distributions of the AS procedure referring to a $25 \times 25\lambda^2$ sized aperture. On the other side, Fig. 13 displays the pattern radiated by the same aperture, but discretized in a 51×51 array with $\lambda/2$ spacing. The mean directivity value has been 26.9 dBi, where the mean

Table 3. Maximum, mean and minimum directivities over the coverage for the aperiodic and periodic reflectarrays designed according to the South America specifications.

Directivity	Aperidoic	Periodic
Maximum	27.25 dBi	27.09 dBi
Mean	26.60 dBi	26.18 dBi
Minimum	25.55 dBi	24.49 dBi

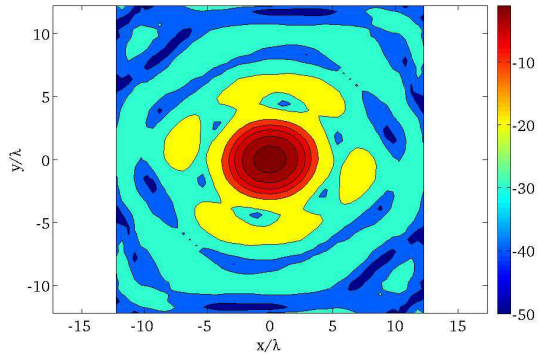

Figure 11. Amplitude distribution of the aperture field for the $25 \times 25\lambda^2$ sized aperture synthesized by the AS scheme according to the South America coverage.

directivity is defined as

$$\frac{1}{\mu(\bar{\Omega})} \iint_{\bar{\Omega}} D(u,v) d\bar{\Omega}, \tag{28}$$

$D(u,v)$ denotes the directivity in the (u,v) direction and $\mu(\bar{\Omega})$ is the measure of $\bar{\Omega}$.

Following this result, the initial positions and phases have been determined according to the procedure in Section 5. These, in turn, lead to the initial radiated pattern displayed in Fig. 14. As it can be seen, the starting point determined according to the mentioned scheme is far from satisfying the coverage requirements. Nevertheless, the APRPOS algorithm is capable to successfully exploit this starting point to synthesize a reflectarray satisfying the design specifications, see Fig. 15. The element positions and control phases corresponding to the pattern in Fig. 15 are reported in Figs. 16 and 17, respectively. The minimum and maximum inter-element spacings have been 0.43λ and 0.7λ, respectively.

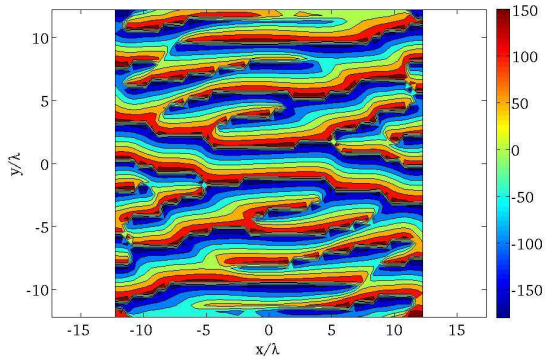

Figure 12. Phase distribution of the aperture field for the $25 \times 25\lambda^2$ sized aperture synthesized by the AS scheme according to the South America coverage.

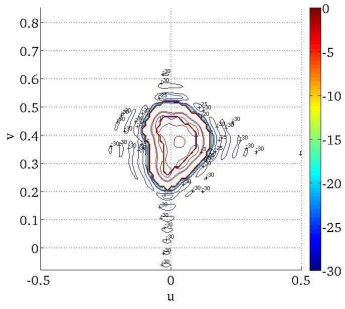

Figure 13. Far-field pattern (along with the mask traces) radiated by the $25 \times 25\lambda^2$ sized aperture synthesized by the AS scheme according to the South America coverage, when discretized in a 51×51 uniform array with $\lambda/2$ spacing.

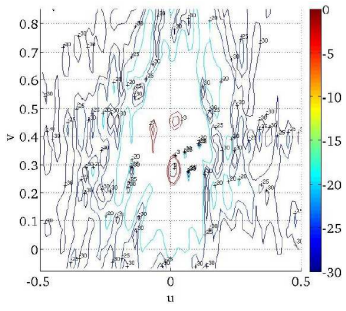

Figure 14. Initial far-field pattern (along with the mask traces) radiated by the 51×51 aperiodic reflectarray obtained from the AS synthesis performed according to the South America coverage and from the procedure of Section 6.

To better appreciate the performance of the synthesized aperiodic reflectarray, we compare the obtained far-field pattern in Fig. 15 to that achievable with a uniform, $\lambda/2$ element spacing, see Fig. 18. The better satisfaction of the coverage requirements of the aperiodic case can be appreciated. This can be even more emphasized by comparing the cuts, along the u- and v-axes, of the far-fields, see Figs. 19 and 20. As

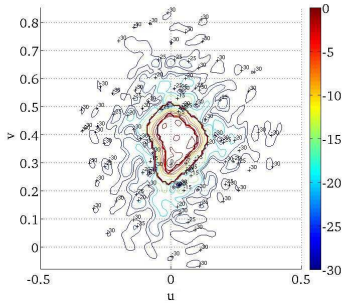

Figure 15. Final far-field pattern (along with the mask traces) radiated by the 51×51 aperiodic reflectarray synthesized according to the South America coverage.

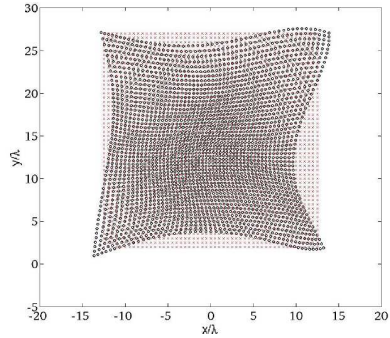

Figure 16. Final element positions for the 51×51 aperiodic reflectarray (black circles) and for a 51×51 periodic reflectarray with $\lambda/2$ spacing (red crosses), both synthesized according to the South America coverage.

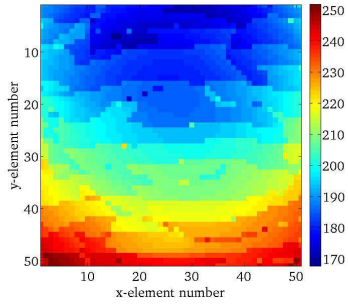

Figure 17. Final control phase distribution for the 51×51 aperiodic reflectarray synthesized according to the South America coverage.

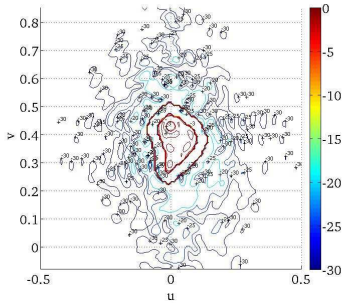

Figure 18. Far-field pattern (along with the mask traces) radiated by the 51×51 periodic reflectarray with $\lambda/2$ synthesized according to the South America coverage.

it can be seen, the aperiodic case reaches lower side-lobes and a more uniform far-field behavior within the coverage. To state again more quantitatively the better performance of the aperiodic reflectarray as compared to the periodic one, we mention that the mean directivities over the coverage for both the cases have been 26.2 dBi and 26 dBi,

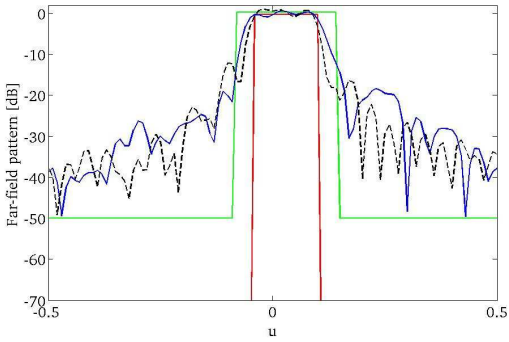

Figure 19. Cut, along the u-axis, of the shaped-beam pattern radiated by the 51×51 aperiodic reflectarray (solid blue line) as compared to the periodic one (dashed black line), both synthesized according to the South America coverage. The green and red line show the upper and lower mask functions, respectively, which have been applied to both the cases.

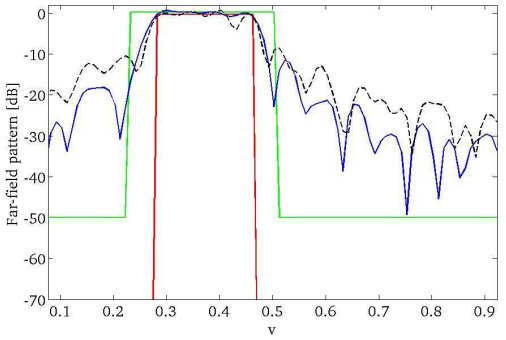

Figure 20. Cut, along the v-axis, of the shaped-beam pattern radiated by the 51×51 aperiodic reflectarray (solid blue line) as compared to the periodic one (dashed black line), both synthesized according to the South America coverage. The green and red line show the upper and lower mask functions, respectively, which have been applied to both the cases.

respectively. However, the root mean square error of the directivity values over the coverage around the mean values have been 0.43 dBi for the aperiodic case and 0.8 dBi for the periodic one. In other words, the far-field pattern for the aperiodic reflectarray has a less varying behavior than that for the periodic one. Furthermore, the performance of the aperiodic reflectarray has a more stable behavior

than the periodic one. Indeed, when reducing the number of elements to 48×48 for both the cases, the mean directivities become 26.0 dBi and 25.6 dBi, respectively. We underline that the mean directivity value of 26.2 dBi achieved by the 51×51-elements aperiodic reflectarray should be considered as a good result, being it very close to the mean directivity value of 26.9 dBi reached by the AS stage. We also would like to stress that the better performance of the aperiodic reflectarray as compared to the periodic one have been obtained even by a slightly smaller overall area (meant as effective scattering area occupied by the elements, and not as final encumbrance of the realized reflectarray as defined by the four tips), as it can be appreciated from Fig. 16. Finally, these results obtained for a single frequency authorize to anticipate that the fully aperiodic reflectarray will have also better performance in terms of frequency variations.

9. CONCLUSIONS AND FUTURE DEVELOPMENTS

A two-stages power pattern technique for the synthesis of flat aperiodic printed reflectarrays, based on the PO radiative model has been presented.

The approach has been conceived to mitigate the typical design issues of reflectarray antennas related to the computational burden and to the possible occurrence of suboptimal solutions which are here even more significant due to the non-regular element lattice. This is done by a convenient, two-stage procedure for choosing the starting point of the iterations and by proper representations of the unknowns of the problem. Design constraints on the element positions have been also accommodated.

The approach has been implemented by parallel programming on GPUs, which has already proven to accelerate computations as compared to standard sequential programming in the framework of aperiodic array antenna analysis [55].

The synthesis technique has been compared against the cases of a pencil-beam and of a shaped-beam involving a typical South America coverage. In both the instances, the performance have outperformed that achievable by the same synthesis procedure, but applied to the case of a periodic radiator.

The method can flexibly accommodate the required specifications in terms of minimum (depending on the considered element type) and maximum allowed spacings. Accordingly, better performance, possibly in terms of bandwidth behavior [64], as compared to that achieved by the presented test cases, could be obtained by relaxing the constraints considered in Section 8.

The method shows a good compromise between accuracy and computational burden. It should be mentioned that the approach can represent a stand-alone synthesis stage, if the reached accuracy can be considered satisfactory, or can represent the core of a more complex reflectarray synthesis strategy, based on a more accurate radiative model and aimed at exploiting all the antenna degrees of freedom [32, 33, 35].

The use of an accurate radiative model [35], the control of the shape of the reflecting surface [36], for which fast analysis tools have been already developed [55], of the orientation of the reflecting elements [36], and the extension to multi-frequency design specifications [36, 61, 62] are already performed continuations of the presented activity. They have been herewith omitted due to lack of space for a thorough discussion, but will be presented in future communications. We finally wish to mention that, taking also into account that in the Authors' experience GPU clusters are becoming even more affordable [65], the implemented computational solution will enable the synthesis of aperiodic (also conformal) reflectarrays of size even larger than the 51×51 herein considered.

ACKNOWLEDGMENT

The authors wish to thank the European Space Agency (ESA) and Space Engineering S.p.A. for the support provided during the LET-SME 2009 ESA activity.

APPENDIX A. THE *REFLECTOR* AND *ARRAY* CONTRIBUTIONS TO THE SCATTERING MATRIX

In this appendix, we briefly sketch how it is possible to identify the *reflector* and *array* contributions to the scattering matrix also in the case of aperiodic arrays.

On supposing to work out a complete coverage of the aperture into cells (see Appendix B), each one corresponding to a different patch (see Fig. B1) and on assuming each cell to be located in the far-zone of F, then the scattering matrix $\underline{\underline{S}}_n$ in Eq. (9) can be expressed as the sum of two contributions as

$$\underline{\underline{S}}_n(u,v) = \underline{\underline{S}}^A_n(u,v) + \underline{\underline{S}}^R_n(u,v), \tag{A1}$$

where $\underline{\underline{S}}^A_n$ is the term due to the n-th patch contribution (in presence of the other ones) and $\underline{\underline{S}}^R_n$ the reflection matrix accounting for the field reflected by a portion of the dielectric slab on the ground plane

(without any patch). The reflector contribution is due to the currents induced, over the ground plane, by the primary field impinging on the dielectric slab leaning on the metallic plate in absence of the patches. More in detail, $\underline{\underline{S}}^R_n$ refers to the ground induced currents restricted to the portion of ground subtended by the n-th patch, according to a proper partitioning, as illustrated in Appendix B (see also Fig. B1).

APPENDIX B. MEAN *REFLECTOR* CONTRIBUTION

In this section, we motivate the reason why, as ground contribution $\underline{\underline{S}}^R_n$ to $\underline{\underline{S}}_n$, a "mean" contribution can be considered, centered around the n-th patch and independently of the patch positions.

We use a Physical Optics approach, evaluating the reflected field $\underline{E}_s$ at the substrate surface (see Fig. 2(b)) by Geometrical Optics, and then calculating the far-field pattern as $\underline{F}(u,v) \propto w\underline{\hat{E}}(u,v)$, $\underline{\hat{E}}$ being the Plane Wave Spectrum (PWS). The PWS can be related to the field $\underline{E}_a$ on the substrate surface as

$$\underline{\hat{E}}(u,v) = \iint_{\mathbb{R}^2} \underline{E}_s(x,y) e^{j\beta(ux+vy)} dxdy. \tag{B1}$$

Of course, in Eq. (B1), the field $\underline{E}_s$ is understood to have support on the substrate surface only, say D.

Under a plane wave incidence, the field $\underline{E}_a$ can be written as

$$\underline{E}_s(x,y) = \underline{\underline{S}}^{R0}\, \underline{E}_f e^{-j\beta(u_0 x+v_0 y)} dxdy \tag{B2}$$

where $\underline{\underline{S}}^{R0}$ is a constant matrix representing the reflection coefficients at the substrate surface and $\underline{E}_f$ contains the only x- and y-components of the impinging plane wave.

According to (B1) and (B2), the PWS can be further expressed as

$$\underline{\hat{E}}(u,v) = \underline{\underline{S}}^{R0}\, \underline{E}_f \iint_{\mathbb{R}^2} f(x,y) e^{-j\beta((u_0-u)x+(v_0-v)y)} dxdy, \tag{B3}$$

where f is the indicator of the domain D.

Let us now introduce a partition of unity $\{f_n\}$ of the domain D, where the functions f_n's are vanishing outside cells, centered around the patch locations, corresponding to a prescribed partitioning of D (for the sake of illustration, in Fig. B1 a partitioning in rectangular tiles is displayed). In other words, each function f_n corresponds to a particular patch indexed by n. Accordingly, in the specular direction (u_0, v_0), the PWS can be rewritten as

$$\underline{\hat{E}}(u_0,v_0) = \underline{\underline{S}}^{R0}\, \underline{E}_f \iint_{\mathbb{R}^2} \sum_n f_n(x,y) dxdy. \tag{B4}$$

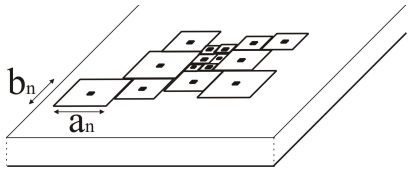

Figure B1. Illustrating the reflectarray surface partitioning by rectangular tiles.

Let us now consider the $\bar{n}$-th patch and translate it, along with the corresponding function, of $(\bar{x}, \bar{y})$. Accordingly, the partition of unity will be changed. Nevertheless, let us observe that the summation in Eq. (B4) can be rewritten as

$$\sum_n f_n(x,y) = \left[f_{\bar{n}}(x-\bar{x}, y-\bar{y}) + \sum_{n\neq\bar{n}} f_n(x,y) \right] + f_{\bar{n}}(x,y) - f_{\bar{n}}(x-\bar{x}, y-\bar{y}). \quad \text{(B5)}$$

The term in square brackets on the right hand side represents a "new" (possibly overlapped) partition corresponding to the new patch positions. The second term, instead, represents the overlap "error". However, since $f_{\bar{n}}(x,y)$ and $f_{\bar{n}}(x-\bar{x}, y-\bar{y})$ subtend the same area, then this error term does not contribute to the integral in Eq. (B4).

Following this observation, when mild aperiodic lattices are considered, it is possible to consider, as ground contribution, that owing to a regular periodic partitioning, which is, from the aperiodic point of view, a "mean" contribution.

We finally observe that:

- in the most realistic case when the impinging field is not a plane wave, the above reasoning holds true in a local sense, whenever the impinging wave can be considered locally plane over subregions of the reflectarray surface; the latter approximation is usually met in practice;
- obviously, we expect that, when evaluating the radiated field along directions different from the specular one owing to the main beam, considering a "mean" ground contribution would lead to errors; however, we observe that, throughout the literature, errors on the lateral lobes are accepted already in well assessed techniques, as the Physical Optics or the P-series approach [63], which are commonly used in antenna synthesis.

REFERENCES

1. Huang, J. and J. A. Encinar, *Reflectarray Antennas*, J. Wiley & Sons, Hoboken, NJ, 2008.
2. Bialkowski, M. E. and J. A. Encinar, "Reflectarrays: Potentials and challenges," *Proc. of the Int. Conf. on Electromagn. in Adv. Appl.*, 1050–1053, Turin, Italy, Sep. 17–21, 2007.
3. Encinar, J. A., M. Arrebola, and G. Toso, "A parabolic reflectarray for a bandwidth improved contoured beam coverage," *Proc. of the Europ. Conf. on Antennas Prop.*, Edinburgh, UK, Nov. 11–16, 2007, CD ROM.
4. Capozzoli, A., C. Curcio, G. D'Elia, and A. Liseno, "Fast phase-only synthesis of conformal reflectarrays," *IET Microw. Antennas Prop.*, Vol. 4, No. 12, 1989–2000, Dec. 2010.
5. Di Maria, A., M. Limbach, R. Horn, and A. Reigber, "Reflectarray membrane study for deployable SAR antenna," *Proc. of the Europ. Conf. on Antennas Prop.*, Berlin, Germany, Mar. 23–27, 2009, CD ROM.
6. Huang, J., "Analysis of a microstrip reflectarray antenna for microspacecraft applications," TDA Progress Report 42-120, Feb. 15, 1995.
7. Fenech, H., A. Tomatis, D. Serrano, E. Lance, and M. Kalama, "Antenna requirements as seen by an operator," *Proc. of the Europ. Conf. on Antennas Prop.*, 3343–3347, Rome, Italy, Apr. 11–15, 2011.
8. Legay, H., B. Salome, E. Labiole, M. A. Milon, D. Cadoret, R. Gillard, R. Chaharmir, and J. Shaker, "Reflectarrays for satellite telecommunication antennas," *Proc. of the Europ. Conf. on Antennas Prop.*, 1–6, Edinburgh, UK, Nov. 11–16, 2007.
9. Willey, R. E., "Space tapering of linear and planar arrays," *IRE Trans. Antennas Prop.*, Vol. 10, No. 4, 369–377, Jul. 1962.
10. Skolnik, M. I., J. W. Sherman III, and F. C. Ogg, Jr., "Statistically designed density-tapered arrays," *IEEE Trans. Antennas Prop.*, Vol. 12, No. 4, 408–417, Jul. 1964.
11. Viganò, M. C., G. Toso, G. Caille, C. Mangenot, and I. E. Lager, "Sunflower array antenna with adjustable density taper," *Int. J. of Antennas Prop.*, Vol. 2009, Article ID 624035, 10 Pages, 2009, doi:10.1155/2009/624035.
12. Donelli, M., A. Martini, and A. Massa, "A hybrid approach based on PSO and Hadamard difference sets for the synthesis of square thinned arrays," *IEEE Trans. Antennas Prop.*, Vol. 57, No. 8, 2491–2495, Aug. 2009.

13. Kurup, D. G., M. Himdi, and A. Rydberg, "Design of an unequally spaced reflectarray," *IEEE Antennas Wireless Prop. Lett.*, Vol. 2, 33–35, 2003.
14. Meriah, S. M., E. Cambiaggio, F. T. Bendimerad, R. Staraj, J. P. Damiano, and L. Brochier, "Design of a thinned microstrip-antenna reflectarray using a genetic algorithm," *Microw. Opt. Tech. Lett.*, Vol. 46, No. 6, 559–562, Sep. 2005.
15. Carrasco, E., M. Barba, and J. A. Encinar, "Switchable-beam reflectarray with aperiodic-gathered elements based on pin diodes," *Proc. of the 32nd ESA Antenna Workshop on Antennas for Space Appl.*, Noordwijk, The Netherlands, Oct. 5–8, 2010, CD ROM.
16. Niaz, M. W., Z. Ahmed, and M. Bin Ihsan, "Performance of thinned microstrip reflectarrays," *IACSIT Int. J. of Eng. and Tech.*, Vol. 2, N. 6, 578–582, Dec. 2010.
17. Capozzoli, A., C. Curcio, A. Liseno, M. Migliorelli, and G. Toso, "Aperiodic conformal reflectarrays," *Proc. of the IEEE Int. Symp. on Antennas Prop.*, 1–4, Spokane, WA, Jul. 3–8, 2011.
18. Capozzoli, A., C. Curcio, A. Liseno, M. Migliorelli, and G. Toso, "Power pattern synthesis of advanced flat aperiodic reflectarrays," *Proc. of the 33rd ESA Workshop on Challenges for Space Antenna Systems*, Noordwijk, The Netherlands, Oct. 18–21, 2011.
19. Zhou, M., S. B. Sorensen, O. S. Kim, S. Pivnenko, and G. Toso, "Investigations on accurate analysis of microstrip reflectarrays," *Proc. of the 33rd ESA Workshop on Challenges for Space Antenna Systems*, Noordwijk, The Netherlands, Oct. 18–21, 2011.
20. Arpin, F., J. Shaker, and D. A. McNamara, "Multi-feed single-beam power-combining reflectarray antenna," *Electronics Letters*, Vol. 40, No. 17, 1035–1037, Aug. 2004.
21. Arrebola, M., J. A. Encinar, and M. Barba, "Multifed printed reflectarray with three simultaneous shaped beams for LMDS central station antenna," *IEEE Trans. Antennas Prop.*, Vol. 56, No. 6, 1518–1527, Jun. 2008.
22. Hajian, M., B. Kuijpers, K. Buisman, A. Akhnoukh, M. Plek, L. C. N. de Vreede, J. Zijdeveld, and L. P. Lightart, "Reconfigurable scan-beam hollow patch reflectarray antenna loaded with tunable capacitor," *Microw. Opt. Tech. Lett.*, Vol. 51, No. 2, 367–374, Feb. 2009.
23. Bucci, O. M., A. Capozzoli, and G. D'Elia, "An effective power synthesis technique for shaped, double-reflector multifeed antennas," *Progress In Electromagnetics Research*, Vol. 39, 93–123, 2003.

24. Huang, J., M. Lou, A. Feria, and Y. Kim, "An inflatable L-band microstrip SAR array," *Proc. of the IEEE Antennas Prop. Int. Symp.*, 2100–2103, Atlanta, GA, Jun. 21–26, 1998.
25. Bucci, O. M., A. Capozzoli, C. Curcio, and G. D'Elia, "On the scattering matrix for reflectarray antennas," *Atti Della Fondazione G. Ronchi*, Vol. LXV, No. 1, 1–17, Jan.–Feb. 2010.
26. Zornoza, J. A. and J. A. Encinar, "Efficient phase-only synthesis of contoured-beam patterns for very large reflectarrays," *Int. J. RF Microw. Computer-aided Eng.*, Vol. 14, No. 5, 415–423, Sep. 2004.
27. Arrebola, M., Y. Álvarez, J. A. Encinar, and F. Las-Heras, "Accurate analysis of printed reflectarrays considering the near field of the primary feed," *IET Microw. Antennas Prop.*, Vol. 3, No. 2, 187–194, 2009.
28. Bucci, O. M., A. Capozzoli, G. D'Elia, and S. Russo, "Power pattern synthesis of reflectarrays: Comparison between two approaches," *Proc. of the XV Riunione Nazionale di Elettromagnetismo*, 1–4, Cagliari, Italy, Sep. 13–16, 2004, CD ROM.
29. Capozzoli, A., A. Colella, C. Curcio, G. D'Elia, A. Liseno, and P. Vinetti, "Constrained phase-only synthesis for reflectarray antennas," *Proc. of the Adv. Lightweight Structures and Refl. Antennas*, Tbilisi, Georgia, Oct. 14–16, 2009, CD ROM.
30. Capozzoli, A., C. Curcio, G. D'Elia, A. Liseno, and P. Vinetti, "FFT & aperiodic arrays with phase-only control and constraints due to super-directivity, mutual coupling and overall size," *Proc. of the 30th ESA Antenna Workshop on Antennas for Earth Observ., Science, Telecomm. and Navig. Space Missions*, Noordwijk, The Netherlands, May 27–30, 2008, CD ROM.
31. Capozzoli, A., C. Curcio, G. D'Elia, A. Liseno, and P. Vinetti, "FFT & equivalently tapered aperiodic arrays," *Proc. of the XXIX General Assembly of the Int. Union of Radio Sci.*, Chicago, IL, Aug. 7–16, 2008, CD ROM.
32. Capozzoli, A., C. Curcio, G. D'Elia, A. Liseno, G. Toso, and P. Vinetti, "Multireflectarray aperiodico conforme," European Patent Nr. 09425356/EP09425356.4, Filing Date: Sep. 16, 2009.
33. Capozzoli, A., C. Curcio, G. D'Elia, A. Liseno, G. Toso, and P. Vinetti, "Aperiodic and non-planar array of electromagnetic scatterers, and reflectarray antenna comprising the same," World Patent Nr. WO/2011/033388, International Filing Date: Sep. 16, 2009.
34. Capozzoli, A., C. Curcio, E. Iavazzo, A. Liseno, M. Migliorelli, and G. Toso, "Phase-only synthesis of a-periodic reflectarrays,"

Proc. of the Europ. Conf. on Antennas Prop., 1031–1035, Rome, Italy, Apr. 11–15, 2011.

35. "Advanced reflectarray antennas," *ESA LET-SME 2009 Project*, Technical Report Nr. 1, Jul. 2010 (Available on Request to the Authors).
36. "Advanced reflectarray antennas," *ESA LET-SME 2009 Project*, Technical Report Nr. 2, Mar. 2011 (Available on Request to the authors).
37. Bulatsyk, O. O., B. Z. Katsenelenbaum, Y. P. Topolyuk, and N. N. Voitovich, *Phase Optimization Problems*, Wiley-VCH Verlag GmbH & Co. KGaA, Weinheim, 2010.
38. Capozzoli, A. and G. D'Elia, "Global optimization and antennas synthesis and diagnostics, part one: Concepts, tools, strategies and performances," *Progress In Electromagnetics Research*, Vol. 56, 195–232, 2006.
39. Capozzoli, A. and G. D'Elia, "Global optimization and antennas synthesis and diagnostics, part two: Applications to advanced reflector antennas synthesis and diagnosis techniques," *Progress In Electromagnetics Research*, Vol. 56, 233–261, 2006.
40. Isernia, T., F. Soldovieri, G. Leone, and R. Pierri, "On the local minima in phase reconstruction algorithms," *Radio Sci.*, Vol. 31, No. 6, 1887–1899, 1996.
41. Bucci, O. M., G. D'Elia, G. Mazzarella, and G. Panariello, "Antenna pattern synthesis: A new general approach," *Proc. of the IEEE*, Vol. 82, No. 3, 358–371, Mar. 1994.
42. Capozzoli, A., C. Curcio, G. D'Elia, and A. Liseno, "Phaseless antenna characterization by effective aperture field and data representations," *IEEE Trans. Antennas Prop.*, Vol. 57, No. 1, 215–230, Jan. 2009.
43. Frieden, B. R., "Evaluation, design and extrapolation methods for optical signals, based on the use of the prolate functions," *Progress in Optics*, E. Wolf, Ed., Vol. 9, 311–407, North-Holland, Amsterdam, 1971.
44. Landau, H. J. and H. O. Pollak, "Prolate spheroidal wave functions, Fourier analysis and uncertainty-III: The dimension of essentially time- and band-limited signals," *Bell Syst. Tech. J.*, Vol. 41, 1295–1336, Jul. 1962.
45. Lebret, H. and S. Boyd, "Antenna array pattern synthesis via convex optimization," *IEEE Trans. Signal Proc.*, Vol. 45, No. 3, 526–532, Mar. 1997.
46. Bucci, O. M., L. Caccavale, and T. Isernia, "Optimal far-field

focusing of uniformly spaced arrays subject to arbitrary upper bounds in nontarget directions," *IEEE Trans. Antennas Prop.*, Vol. 50, No. 11, 1539–1554, Nov. 2002.

47. Boyd, S. and L. Vandenberghe, *Convex Optimization*, Cambridge University Press, Cambridge, 2004.
48. Galindo, V., "Design of dual-reflector antennas with arbitrary phase and amplitude distorsion," *IEEE Trans. Antennas Prop.*, Vol. 12, No. 4, 403–408, Jul. 1964.
49. Dum, D. W. and Y. Rahmat-Samii, "Generalized diffraction synthesis technique for high performance reflector antennas," *IEEE Trans. Antennas Prop.*, Vol. 43, No. 1, 27–40, Jan. 1995.
50. Doyle, W., "On approximating linear array factors," Mem. RM-3530-PR, RAND Coporation, Feb. 1963.
51. Skolnik, M. I., "Nonuniform arrays," *Antenna Theory: Part I*, R. E. Collin and F. J. Zucker, Eds., Ch. 6, McGraw-Hill, New York, 1969.
52. Toso, G. and P. Angeletti, "Sparse and thinned array tracing," European Patent Application No. 08290154.7, Filed on Feb. 18, 2008, Published on Aug. 19, 2009 with the Number EP2090995.
53. Bucci, O. M., M. D'Urso, T. Isernia, P. Angeletti, and G. Toso, "Deterministic synthesis of uniform amplitude sparse arrays via new density taper technique," *IEEE Trans. Antennas Prop.*, Vol. 58, No. 6, 1949–1958, Jun. 2010.
54. Fourmont, K., "Non-equispaced fast Fourier transforms with applications to tomography," *J. Fourier Anal. Appl.*, Vol. 9, No. 5, 431–450, 2003.
55. Capozzoli, A., C. Curcio, G. D'Elia, A. Liseno, and P. Vinetti, "Fast CPU/GPU pattern evaluation of irregular arrays," *Applied Comput. Electromagn. Soc. J.*, Vol. 25, No. 4, 355–372, Apr. 2010.
56. Capozzoli, A., A. Breglia, C. Curcio, and A. Liseno, "GPU-accelerated power pattern synthesis of aperiodic linear arrays," *Proc. of the XXX URSI General Assembly and Scientific Symp.*, 1–4, Istanblu, Turkey, Aug. 13–20, 2011.
57. Pierri, R. and A. Tamburrino, "On the local minima problem in conductivity imaging via a quadratic approach," *Inverse Problems*, Vol. 13, No. 6, 1547–1568, Dec. 1997.
58. Isernia, T., V. Pascazio, and R. Pierri, "On the local minima in a tomographic imaging technique," *IEEE Trans. Geosci. Remote Sens.*, Vol. 39, No. 7, 1596–1607, Jul. 2001.
59. Fatica, M. and W.-K. Jeong, "Accelerating matlab with CUDA," *Proc. of the High Performance Embedded Comput. Workshop*,

Lexington, MA, Sep. 18–20, 2007.

60. Isernia, T., G. Leone, and R. Pierri, "Radiation pattern evaluation from near-field intensities on planes," *IEEE Trans. Antennas Prop.*, Vol. 44, No. 5, 701–710, May 1996.
61. Capozzoli, A., C. Curcio, A. Liseno, M. Migliorelli, and G. Toso, "Phase-only synthesis of conformal aperiodic reflectarrays with multi-frequency specifications," *Proc. of the Europ. Conf. on Antennas Prop.*, Prague, Czech Republic, Mar. 26–30, 2012.
62. Capozzoli, A., C. Curcio, G. D'Elia, A. Liseno, and S. Sparice, "A design technique of reflectarrays with improved frequency performance," *Proc. of the Europ. Conf. on Antennas Prop.*, Edinburgh, UK, Nov. 11–16, 2007.
63. Galindo-Israel, V. and R. Mittra, "A new series representation of the radiation integral with application to reflector antennas," *IEEE Trans. Antennas Prop.*, Vol. 25, No. 5, 631–641, Sep. 1977.
64. Nayeri, P., F. Yang, and A. Z. Elsherbeni, "Broadband reflectarray antennas using double-layer subwavelength patch elements," *IEEE Antennas Wireless Prop. Lett.*, Vol. 9, 1139–1142, 2010.
65. Capozzoli, A., C. Curcio, A. Liseno, and P. V. Testa, "NUFFT-based SAR backprojection on multiple GPUs," *Proc. of the Tyrrhenian Workshop on Advances in Radar and Remote Sens.*, 1–6, Naples, Italy, Sep. 11–14, 2012, CD ROM.